Eur. Phys. J. D **35**, 239–248 (2005)
DOI: 10.1140/epjd/e2005-00193-6

THE EUROPEAN PHYSICAL JOURNAL D

Ab initio and experimental study of the K-shell spectra of *s*-triazine

D. Duflot[1,a], K. Sidhoum[1], J.-P. Flament[1], A. Giuliani[2], J. Heinesch[2], and M.-J. Hubin-Franskin[2,b]

[1] Laboratoire de Physique des Lasers, Atomes et Molécules (PhLAM), UMR CNRS 8523, Centre d'Études et de Recherches Lasers et Applications (CERLA, FR CNRS 2416), Université des Sciences et Technologies de Lille, 59655 Villeneuve d'Ascq Cedex, France

[2] Université de Liège, Laboratoire de Spectroscopie d'Électrons diffusés, Institut de Chimie B6c, Sart Tilman, 4000 Liège 1, Belgium

Received 21 March 2005 / Received in final form 19 May 2005
Published online 26 July 2005 –

Abstract. The carbon and nitrogen K-shell spectra of gaseous *s*-triazine have been studied using inner-shell electron energy loss spectroscopy (ISEELS) method. *Ab initio* Configuration Interaction calculations have been carried out in order to assign the observed bands. As in many similar molecules, both spectra are dominated by an intense π^* peak, followed by lower intensity features. At the C1*s* edge, the calculations show that some previous assignments made using an underestimated core ionisation energy of about 2.5 eV have to be revisited. At the nitrogen edge, the calculations predict a high intensity π^* doubly excited state lying below the ionisation threshold, which could be responsible for one the most intense observable bands at 405.32 eV.

PACS. 31.25.Qm Electron correlation calculations for polyatomic molecules – 34.80.Gs Molecular excitation and ionization by electron impact

1 Introduction

The *s*-triazine molecule and its derivatives are a well-known class of herbicides that are used as photosynthesis inhibitors [1]. Their accumulation in waters, due to their intensive use, has transformed them into pollutants [2] and has raised the question of finding an appropriate treatment for their elimination [3]. Among others, it has been suggested to use photodegradation [4]. To this end, a precise knowledge of the low lying electronic states of the molecule is important. A large number of studies have been devoted to this goal, using both theoretical and experimental methods (see Ref. [5] and references cited therein). Among them, core shell spectroscopy has proven to be a powerful tool for the study of excited states and their characterization as valence or Rydberg character. Due to the localization of the 1s orbitals, this method gives information which are complementary to valence spectroscopies which probe delocalised high-lying orbitals [6].

The *s*-triazine molecule has already been studied using the inner-shell electron energy loss spectroscopy (ISEELS) method by Apen et al. [7], who recorded low resolution (FWHM of 0.6 eV) spectra and assigned the spectral bands by comparison with similar molecules, such as pyridine or benzene. Since our previous works on these molecules [8,9] have led to reconsider some assignments, it seems worthwhile to reconsider the core spectra of *s*-triazine.

The goal of the present paper is to present a new ISEELS spectrum of *s*-triazine recorded with a resolution of 0.17 eV. In order to help in the assignment of the observed spectral features, *ab initio* calculations using Configuration Interaction (CI) calculations have been carried out. This paper is divided into the following sections: Section 2 describes the experimental set-up; Section 3 deals with the computational method employed; the results are presented and discussed in Section 4 and finally, in Section 5 some conclusions are given.

2 Experiment

The inner-shell electron energy loss spectra were obtained with a VSW spectrometer which has been adapted for gas studies and high energy electron beams and has been equipped with a home-made position sensitive multi-detector system in order to improve data collection times. The experimental apparatus and procedure have been described in detail previously [10,11].

Briefly the spectrometer consists of an electrostatic 180° monochromator operating in the constant pass energy mode, a collision chamber and an electrostatic

[a] e-mail: denis.duflot@univ-lille1.fr
[b] Directeur de recherche F.N.R.S.

analyser identical to the monochromator. The monochromatised incident electrons are accelerated up to 2 keV and focused into the collision chamber using a four-element electron lens. The electrons are slightly deflected (0.02 radians) by two sets of X-Y plates inside the collision chamber. The scattered electrons are energy analyzed and focused onto the entrance slit of the analyser by a lens similar to that used for acceleration.

In the collision conditions of low momentum transfer (i.e. high incident energy and small scattering angle), electronic electric-dipolar transitions are primarily excited.

Inside the vacuum vessel, a residual pressure of less than 1×10^{-8} Torr is maintained by a cryogenic pumping system. The electron gun and the analyser regions are differentially pumped by turbomolecular pumps respectively.

The detection system consists of an assembly of two microchannel plates, a phosphor screen, fiber-optic couplers and an area array Coupled Charge Device (CCD) sensor. The driving and reading electronics for the detector have been adapted to the electron-energy loss experiment. The spectra result from the accumulation of the data from each channel of the detector, which removes any detector-sensitivity variation [10,12].

The accelerating and retarding voltages were constant to within 10 ppm/°C. The spectra have been recorded with 0.040 eV steps. At the C1s and N1s edges the regions containing fine features not well resolved have been recorded with smaller steps 0.020 eV and 0.010 eV in order to determine more accurately the corresponding energy values.

In order to take into account valence and lower-energy inner-shell excitation cross section, a background has been subtracted from the raw spectra by extrapolating a least-square fit of the pre-edge experimental data points. The absolute energy scales were determined by calibrating the C1s spectrum relative to the C1$s \rightarrow \pi^*$ ($\nu' = 0$) band in CO [13] at 287.40 ± 0.02 eV and the N1s spectrum relative to the N1$s \rightarrow \pi^*$ ($\nu' = 0$ and $\nu' = 1$) band for N_2 (i.e. 401.10 eV which is the average value of $\nu' = 0$ and $\nu' = 1$ as the features due to these transitions are only partly resolved within our 0.17 eV resolution [13]). The spectrum of a mixture of s-triazine and the calibration gas (CO or N_2) was recorded with each gas being let into the collision region through a separate leak to ensure of constant composition mixture. The uncertainty on the measured energies is of the order of 0.06 eV and 0.13 eV for the C1s and N1s spectra, respectively.

The sample is a commercial one from ALDRICH with a stated purity of 97.0%. It was used directly without further purification except for repetitive freeze-pump-thaw cycles in order to eliminate air and other volatile impurities in the sample.

3 Computational method

Since the computational method used has been described in detail elsewhere [14], it will be briefly outlined. The starting hypothesis [15] is that, due to the important relaxation of the electronic density following the creation of the core hole, the molecular orbitals (MO's) of the core *ionised* molecule are a better approximation for the description of the core *excited* states than the ground state MO's. Similarly, the energy of a given $1s \rightarrow i^*$ core excited state may be obtained by correcting the core ion energy in the following manner:

$$E(1s \rightarrow i^*) = E(1s \rightarrow \infty) + \varepsilon_{i*} + P + C$$

where ε_{i^*} is the Hartree-Fock mono-electronic energy of the i^* MO. $E(1s \rightarrow \infty)$ is the MP2 core ion energy, obtained using the ROHF-GVB method implemented in the GAMESS-US package [16]. The P and C terms represent the residual relaxation and valence correlation effects of the i^* electron with respect to the core ion, respectively. P is obtained by performing a configuration interaction (CI) calculation in the mono-excitation space of all the calculated $1s \rightarrow i^*$ states. In order to evaluate the C term, the resulting CI wave-functions serve as the zeroth-order space for a multi-reference MP2 calculation using the three-class diagrammatic CIPSI method [17]. To spare computational time, an extrapolation procedure [18] was employed, using 6 thresholds between 99.4 and 99.9% of the exact wave functions. Finally, the dipolar electric transition oscillator strengths with respect to the ground state of the molecule were computed, using the length gauge.

The s-triazine molecule contains three chemically equivalent carbon and nitrogen atoms. For the calculation of the core ionised MO's at both edges, core hole localisation was assumed and the coupling between excitations from different core holes was neglected. Thus, the molecular symmetry was reduced from D_{3h} to C_{2v}. In the following, the core excited carbon and nitrogen atoms will be noted as C_e and N_e, respectively. Finally, the Gaussian atomic orbitals (AO's) used are the TZP basis set taken from Dunning [19]. For the calculation of the core-excited states, a set of Rydberg orbitals (5s, 5p, 2d) was added at the centre of the molecule. The first exponents were taken from Dunning and Hay [20] and the last ones were determined in an "even-tempered" manner.

Finally, in order to interpret the width of the first band at both edges, Franck-Condon factors calculations were carried out, using the method proposed by Cederbaum and Domcke [21]. Using the linear coupling approximation, this model requires the determination of the gradient (the κ-matrix) of the core excitation energy at the ground state geometry:

$$\kappa_i = 2^{-1/2} \left(\frac{\partial E_v}{\partial Q_i} \right)_0 .$$

The κ-matrix and the unscaled harmonic frequencies of the ground state were evaluated at the HF level. In the present work, the calculations included hot bands as well as combination bands. The theoretical width of the vibrational bands was set to the experimental resolution (0.17 eV) and Gaussian profile was used.

Table 1. Calculated geometry of *s*-triazine compared with previous works (bond lengths in Å and angles in degrees).

	RHF[a]	MP2[a]	CASSCF[b]	B3LYP[b]	RHF[c]	Exp.[d]	Exp.[e]	Exp.[f]
	TZP	TZP	6-31G*	6-31G*	TZVP	ED	Raman	X-ray
r(C-N)	1.3158	1.3372	1.328	1.337	1.3154	1.338(1)	1.338	1.317
r(C-H)	1.0736	1.0810	1.073	1.089	1.0739	1.106(8)	(1.084)[g]	1.045
HCN	117.3	117.0				116.9	116.6	114.8
NCN	125.4	126.0			125.5	126.1	127.0	125.2
CNC	114.6	114.0				113.9(1)	113.2	

[a] This work, [b] Ref. [5], [c] Ref. [25], [d] Ref. [24], [e] Ref. [23], [f] Ref. [22], [g] value fixed arbitrarily.

Table 2. Core ionisation energies (eV) of *s*-triazine.

	C1s	N1s
ΔSCF[a]	294.15	405.70
ΔMP2[a]	293.28	406.14
Experiment[b]	290.6	404.9

[a] This work. Energies calculated using the TZP+Rydberg basis set at the MP2/TZP optimised geometry. [b] Estimated values from reference [7] based on like materials from reference [26].

4 Results and discussion

The HF electronic configuration of the neutral ground state of *s*-triazine is:

$$1e'^4 1a_1'^2 2e'^4 2a_1'^2 3a_1'^2 3e'^4 4e'^4 4a_1'^2 1a_2'^2 1a_2''^2 5e'^4 5a_1'^2 1e''^4 6e'^4.$$

The six first MO's are the 1s orbitals of the nitrogen and carbon atoms. The $1a_2''$ MO is the lowest π orbital (1π). The $1e''$ MO corresponds to the 2π and 3π (degenerate) orbitals. Their anti-bonding counterparts are the $2e''$ and the $2a_2''$ ones, respectively. In the C_{2v} symmetry point group of the core excited species, the $2e''$ MO generates the $3b_1$ ($1\pi^*$) and the $2a_2$ ($2\pi^*$) MO's, while the $2a_2''$ becomes the $4b_1$ ($3\pi^*$) MO. In the D_{3h} symmetry group, corresponding to the true symmetry of the molecule (or a delocalised core hole), the transitions from the $1s(1e')$ MO's to a_1'' and a_2'' MO's are dipole electric forbidden; for the $(1s)1a_1'$ MO, only transitions to a_2'' and e' MO's are dipole electric allowed. In the C_{2v} group, corresponding to the localised picture used for the calculations, all electronic transitions are dipole allowed except $1s \rightarrow 2\pi^*(2a_2)$. The MP2 optimised D_{3h} geometry of the ground state of *s*-triazine compares well with previous experimental [5,22–24] and theoretical works [25], as shown in Table 1. Thus, all the calculations were carried out at this geometry.

The calculated core ionisation energies, obtained at the RHF and MP2 levels, are shown in Table 2. In the absence of any experimental determination of these quantities, Apen et al. [7] used the values of like materials taken from a compilation [26]. Since, according to our previous work [27], the calculated values should be accurate within a few tenths of an eV, it appears that the values of 290.6 eV for the C1s ionisation energy is underestimated by several eV. This will have some consequences on the assignment of the carbon K-shell spectrum (see below). The N1s ionisation energy appears to be also underestimated by about 1 eV.

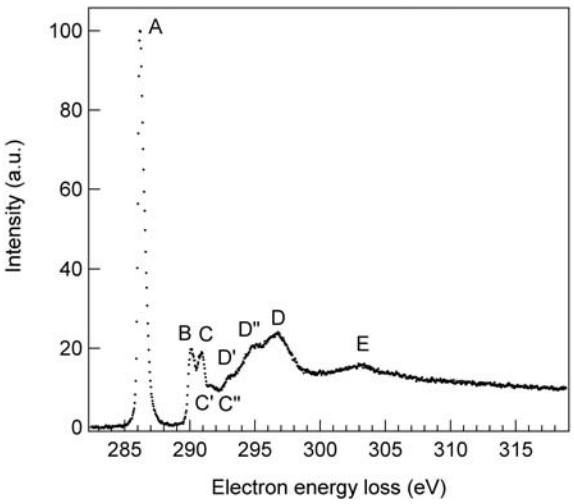

Fig. 1. The electron energy loss spectrum of *s*-triazine recorded at the carbon K edge with an energy resolution of 0.17 eV.

4.1 Carbon K-shell electron-energy loss spectrum

The measured carbon K-shell energy loss spectrum of *s*-triazine is displayed in Figure 1. The spectrum is similar to that obtained by Apen et al. [7] at low resolution (0.6 eV) but the better resolution of the present work allows to distinguish more details. Globally, the energies of the observed bands are in agreement with those of Apen et al. [7], as shown in Table 3. The table also provides the assignments initially proposed in reference [7]. The results of the calculations are given in Table 4.

The first band A is observed at 286.16 eV and is assigned without ambiguity to the $1s \rightarrow 1\pi^*$ ($1e''$, $3b_1$) transition, which is calculated to occur at 286.32 eV (Tab. 4). This band has a FWHM of 0.57 eV, close to the 0.55 eV value reported by Apen et al. [7]. The band is asymmetric in the high energy region, which suggests possible vibrational excitation. The calculated vibrational structure is displayed in Figure 2a. The vertical transition was set to the calculated value of 286.32 eV. Although the calculated width is too small, the asymmetry is correctly reproduced. The vibrational progression is dominated by the 0–0 transition. This peak is followed by four medium

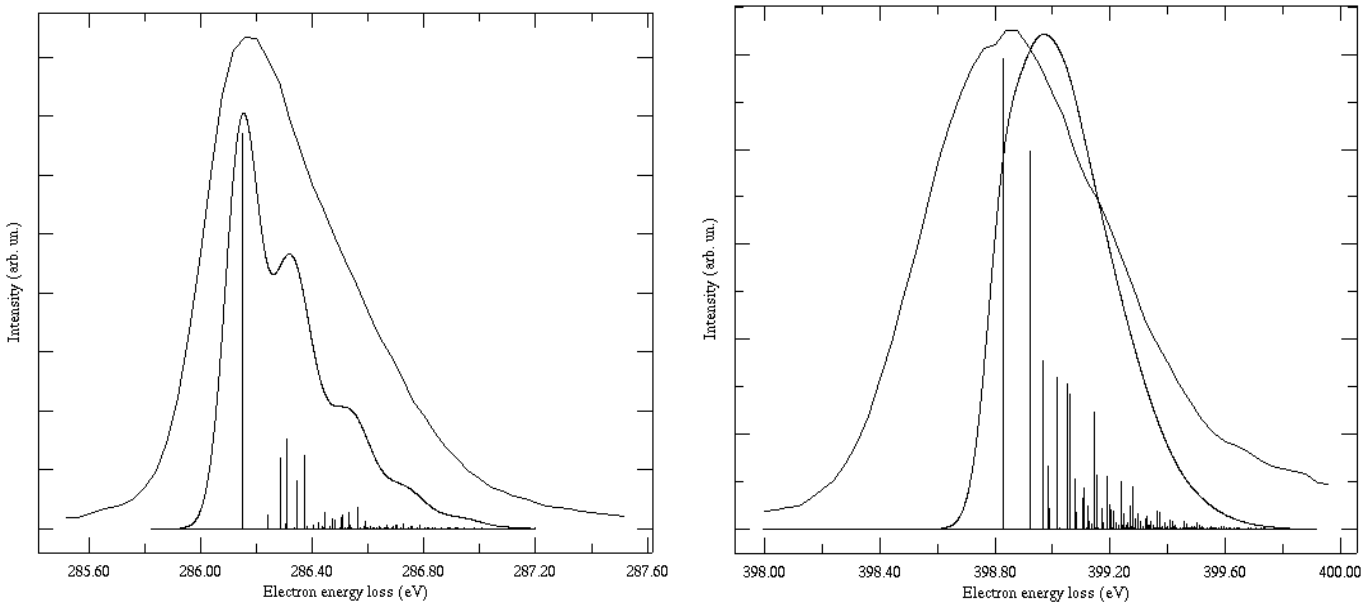

Fig. 2. Calculated vibrational structure of the first bands. (a) C1s edge; (b) N1s edge.

Table 3. Measured energies (eV) of the spectral features in the C1s spectrum and previous proposed assignments.

	E (eV)[a]	E (eV)[b]	Assignment[b]
A	286.16	286.2	$1\pi^*$ $(2e'')$
		287.5	
B	290.09	290.1	$3\pi^*$ $(2a_2'')$
	(290.64)		
C	290.84	290.8	σ^*(C–H)
	(291.22)		
C'	291.58		
C"	292.02	(292)	double excitation
D'	293.08	(293)	double excitation
		(294)	double excitation
D"	295.12		
D	296.66	296.5	σ^*(C–N)
E	303.36	303.0	σ^*(C–N)

[a] This work. Not well resolved features are given in parentheses, [b] Ref. [7].

intensity peaks corresponding to excitation of the carbon-nitrogen ring modes. This suggests that the geometry of the $1s \rightarrow 1\pi^*$ state should be close to the ground state one. This is confirmed by a geometry optimisation of this state (at HF level): the molecule remains planar; the ring is slightly distorted with the C_eN distance reduced to 1.2806 Å.

Apen et al. [7] also reported a low intensity feature at 287.5 eV, without giving any assignment. This feature does not seem to be present in the present spectrum (Fig. 1) but, according to the calculations, the $1s \rightarrow 2\pi^*(1e'', 2a_2)$ dipole electric forbidden transition is predicted to occur at 286.98 eV. However, its calculated electric quadrupole oscillator strength is negligible.

The next band B is observed at 290.09 eV with a not well resolved feature at 290.64 eV (Tab. 3). Apen et al. [7] assigned it to the $1s \rightarrow 3\pi^*(2a_2'', 4b_1)$ transition, by analogy with the pyridine case [28]. However, it has to be assigned to the $1s \rightarrow 3s\sigma/\sigma^*(C_e$–H) which is predicted to occur by the calculations at 289.83 eV (Tab. 4). Its rather large intensity (6.4% of the first peak) is due to the large $\sigma^*(C_e$–H) valence character of the $3s\sigma$ MO. This trend is very frequent in the carbon K-shell spectra of organic molecules [8–27].

The B band is also asymmetric in the high energy side, probably because of vibrational excitation, and overlaps partially with the C band, whose maximum is measured at 290.84 eV with a not well resolved feature at 291.22 eV. This band was assigned by Apen et al. [7] to a $1s \rightarrow \sigma^*$(C–H) transition and was supposed to lie at the continuum onset, assuming a ionisation energy of 290.6 eV. In fact it is mainly due to a $1s \rightarrow 3p\sigma/\sigma^*(C_e$–H) valence-Rydberg transition, calculated at 290.56 eV, and to a rather intense (12.8%) π^* (b_1) transition predicted at 290.73 eV (Tab. 4). Although the calculated wave-function appears to be strongly mixed (Tab. 4), this state is assigned to the $3\pi^*$ transition.

The next energy region of the spectrum between 291 and 293 eV does not present any clear feature, except possible not well resolved structures at C' at 291.58 eV and C" at 292.02 eV. As shown in Table 4, the transitions calculated in this energy range correspond to Rydberg states ($n = 3$–7) and have very small intensities. Two states of particular interest are calculated at 291.83 and 291.85 eV. Their wave-functions are strongly mixed: the first one is dominated by valence di-excitations with a

Table 4. Calculated energies, TV's, relative intensities and assignments of C1s core excited states of *s*-triazine.

State	E(eV)	TV(eV)	Intensity[a]	Main configurations	$\langle r^2 \rangle$
B_1	286.32	6.96	1.000	0.92 $1s \rightarrow 1\pi^*$	79
A_2	286.98	6.30	0.000[b]	0.92 $1s \rightarrow 2\pi^*$	80
A_1	289.83	3.45	0.064	0.95 $1s \rightarrow 3s\sigma/\sigma^*(C_e\text{–H})$	128
B_1	290.45	2.83	0.008	0.74 $1s \rightarrow 3p\pi$	128
				+ 0.12 $1s \rightarrow 3\pi^*$	
A_1	290.56	2.72	0.053	0.94 $1s \rightarrow 3p\sigma/\sigma^*(C_e\text{–H})$	145
B_1	290.73	2.55	0.128	0.35 $1s \rightarrow 3\pi^*$	134
				+ 0.22 $1s \rightarrow 3p\pi$	
				+ 0.11 $1s \rightarrow 3d\pi$	
				+ 0.10 $1s2\pi \rightarrow 1\pi^*1\pi^*$	
B_2	290.88	2.40	<0.001	0.97 $1s \rightarrow 3p\sigma$	195
A_1	291.23	2.06	0.002	0.95 $1s \rightarrow 3d\sigma$'	180
B_2	291.43	1.85	0.004	0.97 $1s \rightarrow 3d\sigma$	200
A_1	291.47	1.82	0.004	0.95 $1s \rightarrow 3d\sigma$	225
B_1	291.51	1.77	<0.001	0.84 $1s \rightarrow 3d\pi$	220
A_2	291.60	1.68	0.000[b]	0.98 $1s \rightarrow 3d\pi$	232
A_1	291.70	1.59	0.017	0.95 $1s \rightarrow 4s\sigma/\sigma^*(C_e\text{–H})$	400
B_1	291.83	1.45	0.010	0.39 $1s2\pi \rightarrow 1\pi^*1\pi^*$	261
				+ 0.36 $1s \rightarrow 4d\pi$	
				+ 0.13 $1s3\pi \rightarrow 1\pi^*2\pi^*$	
B_1	291.85	1.43	0.004	0.58 $1s \rightarrow 4d\pi$	500
				+ 0.14 $1s2\pi \rightarrow 1\pi^*1\pi^*$	
				+ 0.12 $1s3\pi \rightarrow 1\pi^*2\pi^*$	
B_1	291.88	1.41	0.039	0.82 $1s \rightarrow 4p\pi$	463
A_1	291.93	1.35	0.019	0.95 $1s \rightarrow 4p\sigma$	490
B_2	292.02	1.26	0.000	0.96 $1s \rightarrow 4p\sigma$	734
A_1	292.08	1.20	<0.001	0.96 $1s \rightarrow 4d\sigma$	688
B_2	292.14	1.14	0.002	0.97 $1s \rightarrow 4d\sigma$	617
A_1	292.16	1.12	<0.001	0.95 $1s \rightarrow 4d\sigma$'	715
A_2	292.20	1.09	0.000[b]	0.98 $1s \rightarrow 4d\pi$	598
A_1	292.26	1.02	0.010	0.94 $1s \rightarrow 5s\sigma$	966
B_1	292.31	0.97	0.005	0.93 $1s \rightarrow 5p\pi$	1231
B_2	292.34	0.94	<0.001	0.96 $1s \rightarrow 5p\sigma$	1091
A_1	292.35	0.93	0.005	0.86 $1s \rightarrow 5p\sigma$	1058
A_1	292.53	0.75	<0.001	0.89 $1s \rightarrow 6s\sigma$	3555
A_1	292.66	0.62	0.001	0.97 $1s \rightarrow 6p\sigma$	7724
B_2	292.66	0.62	<0.001	0.98 $1s \rightarrow 6p\sigma$	7690
B_1	292.66	0.62	<0.001	0.98 $1s \rightarrow 6p\pi$	7746
A_1	292.77	0.51	<0.001	0.98 $1s \rightarrow 7s\sigma$	>10000
A_1	292.83	0.45	<0.001	0.98 $1s \rightarrow 7p\sigma$	>10000
B_2	292.83	0.45	<0.001	0.98 $1s \rightarrow 7p\sigma$	>10000
B_1	292.83	0.45	<0.001	0.98 $1s \rightarrow 7p\pi$	>10000
A_1	293.07	0.21	0.089	0.94 $1s \rightarrow \sigma^*(C_e\text{–H})$	179
	293.28	0.00		ion	
B_2	293.80	–0.52	0.059	0.94 $1s \rightarrow \sigma^*$(C–N)	129
A_1	293.86	–0.58	0.004	0.95 $1s \rightarrow \sigma^*$(C–N)	125
A_1	294.91	–1.62	<0.001	0.54 $1s\ 2\pi \rightarrow 1\pi^*\ 3s\sigma/\sigma^*(C_e\text{–H})$	134
B_2	294.93	–1.64	0.031	0.95 $1s \rightarrow \sigma^*$	101
A_1	295.50	–2.22	<0.001	0.63 $1s\ 2\pi \rightarrow 3\pi^*\ 3p\sigma/\sigma^*(C_e\text{–H})$	186
B_2	296.12	–2.84	<0.001	0.63 $1s\ 2\pi \rightarrow 1\pi^*\ 3p\sigma$	209

[a] Relative intensity to the most intense peak. The absolute calculated oscillator strength of the first transition is $f = 0.0577$,
[b] forbidden dipole electric transition.

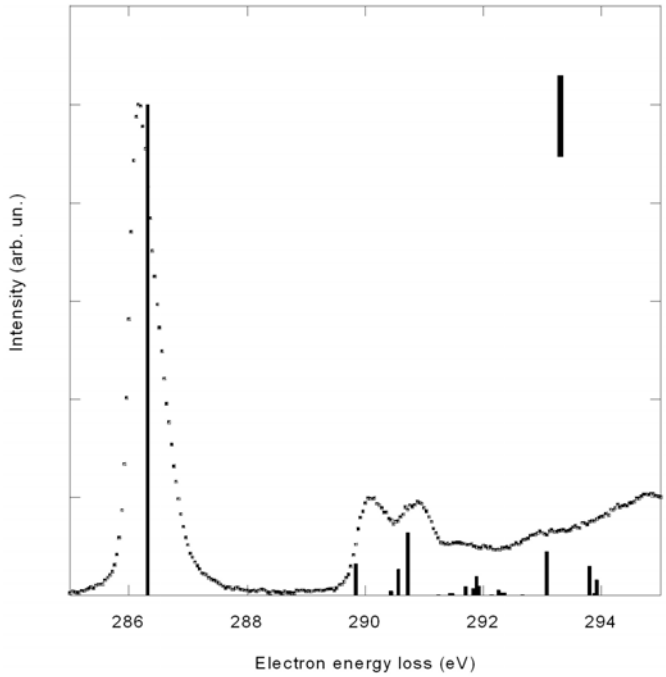

Fig. 3. Comparison of the calculated C1s spectrum with the experimental one. The vertical line indicates the calculated ionisation threshold.

substantial $4d\pi$ character, while the situation is reversed for the second one. The $\langle r^2 \rangle$ values of the first one (261 a.u.^{2}) is too low to assign it to an $n = 4$ Rydberg state. The $\langle r^2 \rangle$ values of the first one (500 a.u.^{2}) is higher and is compatible with an $n = 4$ Rydberg state. Thus, we qualitatively assign the first state to a valence di-excited state and the second to the $4d\pi$ Rydberg transition.

The feature D' observed at 293.08 eV was assigned by Apen et al. [7] to a double excitation state, since it was supposed to lie well above the ionisation threshold. In fact, it should correspond to the continuum onset if the calculated ionisation energy of 293.28 eV is correct. Moreover, the calculations predict the $1s \rightarrow \sigma^*(C_e\text{–H})$ transition to occur at 293.07 eV (Tab. 4) with a rather large intensity (8.9%). Therefore, the calculations confirm that the $\sigma^*(C_e\text{–H})$ transition is quasi-degenerate with the continuum onset, but about 2.5 eV higher than proposed by Apen et al. [7].

The last three features observed in the spectrum (D" at 295.12 eV, D at 296.66 eV and E at 303.36 eV) are above the ionisation threshold (Tab. 3). The calculations of Table 4 predict several states above the edge, including excitations to σ^* orbitals as well as di-excited states. However, these results cannot be considered as quantitative since the influence of the continuum is not taken into account. Moreover, the observed bands are too high in energy to be calculated. These three bands are tentatively assigned to shape resonances but it should be kept in mind that this type of assignment has been questioned [29].

The synthetic spectrum resulting from the calculations is compared with the experimental spectrum in Figure 3.

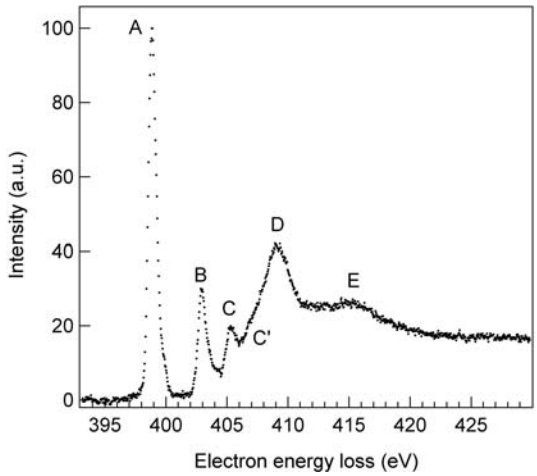

Fig. 4. The electron energy loss spectrum of s-triazine recorded at the nitrogen K edge with an energy resolution of 0.17 eV.

Table 5. Measured energies (eV) of the spectral features in the N1s spectrum and previous proposed assignments.

	E (eV)[a]	E (eV)[b]	E (eV)[c]	Assignment[b]
A	398.84	398.8	399.9	$1\pi^*$ $(2e'')$
	(402.36)			
B	402.92	402.9	404.2	$3\pi^*$ $(2a_2'')$
	(403.24)			
	(403.44)			
	(403.60)			
B'	404.12			
C	405.32	405.5	406.8	double excitation/ continuum onset
C'	406.84			
D	409.10	409.2	409.6	σ^*(C–N)
E	415	415.3	417.5±1	σ^*(C–N)

[a] This work. Not well resolved features are given in parentheses, [b] Ref. [7], [c] Ref. [30].

It appears that the theoretical energies are accurate within a few tenths of an eV.

4.2 Nitrogen K-shell electron-energy loss spectrum

The measured nitrogen K-shell energy loss spectrum of s-triazine is shown in Figure 4 and the energies of the observed bands are given in Table 5. As for the carbon case, the results are in good agreement with those obtained at low resolution by Apen et al. [7]. Table 5 also displays the results obtained by Dudde et al. [30] on condensed thick films of s-triazine. These values appear to be too large by about 1 eV when compared to the two gas phases studies, possibly because of a calibration error as suggested by Apen et al. [7]. The results of the present calculations are given in Table 6.

Table 6. Calculated energies, TV's, relative intensities and assignments of N1*s* core excited states of *s*-triazine.

State	E(eV)	TV(eV)	Intensity[a]	Main configurations	$\langle r^2 \rangle$
B_1	399.05	7.09	1.000	0.91 $1s \rightarrow 1\pi^*$	79
A_2	399.69	6.45	0.000[b]	0.93 $1s \rightarrow 2\pi^*$	80
A_1	402.76	3.38	<0.001	0.97 $1s \rightarrow 3s\sigma$	127
B_1	403.43	2.71	0.093	0.91 $1s \rightarrow 3p\pi$	142
A_1	403.66	2.48	0.020	0.96 $1s \rightarrow 3p\sigma$	176
B_2	403.66	2.48	<0.001	0.98 $1s \rightarrow 3p\sigma$	182
B_1	404.03	2.11	0.116	0.46 $1s \rightarrow 3d\pi$	186
				+ 0.20 $1s \rightarrow 3\pi^*$	
				+ 0.16 $1s \rightarrow 4p\pi$	
A_1	404.06	2.08	0.007	0.95 $1s \rightarrow 3d\sigma$	176
B_1	404.10	2.04	0.152	0.52 $1s \rightarrow 3d\pi$	195
				+ 0.18 $1s \rightarrow 3\pi^*$	
				+ 0.15 $1s \rightarrow 4p\pi$	
A_1	404.28	1.86	0.002	0.95 $1s \rightarrow 3d\sigma$	201
B_2	404.36	1.78	0.005	0.97 $1s \rightarrow 3d\sigma$'	220
A_2	404.45	1.69	0.000[b]	0.98 $1s \rightarrow 3d\pi$	231
A_1	404.58	1.56	<0.001	0.97 $1s \rightarrow 4s\sigma$	423
B_1	404.62	1.52	0.042	0.65 $1s \rightarrow 4p\pi$	513
				+ 0.20 $1s \rightarrow 3\pi^*$	
A_1	404.84	1.30	0.012	0.72 $1s \rightarrow 4p\sigma$	557
				+ 0.20 $1s \rightarrow 4d\sigma$	
B_2	404.86	1.28	<0.001	0.97 $1s \rightarrow 4p\sigma$	628
A_1	404.92	1.22	0.001	0.72 $1s \rightarrow 4d\sigma$	684
				+ 0.24 $1s \rightarrow 3p\sigma$	
A_1	405.00	1.14	0.001	0.93 $1s \rightarrow 4d\sigma$'	624
B_2	405.02	1.12	0.003	0.97 $1s \rightarrow 4d\sigma$	771
B_1	405.04	1.10	0.003	0.97 $1s \rightarrow 4d\pi$	617
A_2	405.05	1.09	0.000[b]	0.98 $1s \rightarrow 4d\pi$	600
A_1	405.12	1.02	<0.001	0.93 $1s \rightarrow 5s\sigma$	875
B_1	405.15	0.99	0.007	0.90 $1s \rightarrow 5p\pi$	1221
B_2	405.20	0.94	0.001	0.97 $1s \rightarrow 5p\sigma$	1036
A_1	405.21	0.93	0.007	0.88 $1s \rightarrow 5p\sigma$	1148
A_1	405.38	0.76	0.001	0.93 $1s \rightarrow 6s\sigma$	3597
B_1	405.51	0.63	<0.001	0.98 $1s \rightarrow 6p\pi$	7745
B_2	405.52	0.62	<0.001	0.98 $1s \rightarrow 6p\sigma$	7693
A_1	405.52	0.62	<0.001	0.98 $1s \rightarrow 6p\sigma$	7728
A_1	405.63	0.51	<0.001	0.99 $1s \rightarrow 7s\sigma$	>10000
B_2	405.69	0.45	<0.001	0.99 $1s \rightarrow 7p\sigma$	>10000
B_1	405.69	0.45	<0.001	0.99 $1s \rightarrow 7p\pi$	>10000
A_1	405.69	0.45	<0.001	0.99 $1s \rightarrow 7p\sigma$	>10000
B_1	405.89	0.25	0.163	0.13 $1s \rightarrow 3\pi^*$	92
				+ 0.52 $1s\ 3\pi \rightarrow 1\pi^*\ 2\pi^*$	
				+ 0.18 $1s\ 2\pi \rightarrow 2\pi^*\ 3p\pi$	
B_1	405.94	0.20	<0.001	0.67 $1s\ 2\pi \rightarrow 1\pi^*\ 1\pi^*$	79
				+ 0.19 $1s\ 3\pi \rightarrow 1\pi^*\ 2\pi^*$	
	406.14	0.00		ion	
A_1	406.26	–0.12	0.025	0.87 $1s \rightarrow \sigma^*$(C–H)	142
B_2	406.71	–0.57	0.132	0.95 $1s \rightarrow \sigma^*$(C–H)	131
A_1	406.72	–0.58	0.017	0.85 $1s \rightarrow \sigma_1^*$	123
B_2	407.87	–1.73	0.078	0.97 $1s \rightarrow \sigma_1^*$	99
B_2	407.89	–1.75	0.038	0.37 $1s \rightarrow \sigma_2^*$	171
				+ 0.50 $1s\ 3\pi \rightarrow 1\pi^*\ 3p\sigma$	
A_1	407.93	–1.79	<0.001	0.80 $1s\ 3\pi \rightarrow 2\pi^*\ 3s\sigma$	138
A_1	408.52	–2.38	0.037	0.55 $1s \rightarrow \sigma_4^*$	149
				+ 0.30 $1s\ 3\pi \rightarrow 3\pi^*\ 3p\sigma$	
B_2	408.57	–2.43	0.067	0.54 $1s \rightarrow \sigma_3^*$	148
				+ 0.33 $1s\ 3\pi \rightarrow 1\pi^*\ 3p\sigma$	
A_1	408.59	–2.45	0.026	0.37 $1s \rightarrow \sigma_4^*$	163
				+ 0.45 $1s\ 3\pi \rightarrow 2\pi^*\ 3p\sigma$	

[a] Relative intensity to the most intense peak. The absolute calculated oscillator strength of the first transition is $f = 0.0294$.
[b] Forbidden dipole electric transition.

As for C1s threshold, the first band A, observed at 398.84 eV with a FWHM of 0.77 eV, corresponds to the N1$s \rightarrow 1\pi^*$ ($2e''$, $3b_1$) transition, calculated at 399.05 eV (Tab. 6). This band is asymmetric in the high energy range and there seems to be a not well resolved feature around 399.9 eV, in the high energy tail of the A band. Its energy seems too large to assign it to vibrational excitation of the A band. This is confirmed by the calculation of the vibrational structure, which is compared to the experiment in Figure 2b. As for the C1s case, the theoretical width is too small but the asymmetry is reproduced. The vibrational structure is also dominated by the 0–0 transition, with excitation of the ring modes. Vibrational excitation appears to be more important than for the C1s case. Optimisation of the geometry of this state at the HF level shows that it remains planar, with an important distortion of the ring: the N_eC is practically unchanged (1.3170 Å), the next CN bonds are shortened (1.2792 Å) and the last NC bonds (where C is opposite to N_e) is increased (1.3307 Å). The CH bonds are unchanged.

The electric dipole forbidden $1s \rightarrow 2\pi^*(1e'', 2a_2)$ transition is calculated at 399.69 eV (Tab. 6). This suggests a possible electric quadrupole transition for the 399.9 eV feature. However, the corresponding calculated oscillator strength was found to be negligible.

The next band B in the spectrum is centred at 402.92 eV with not well resolved fine features at 402.36, 403.24, 403.44 and 403.60 eV (Fig. 4). This band was assigned by Apen et al. [7] to the $1s \rightarrow 3\pi^*$ ($2a_2''$, $4b_1$) transition by analogy with the pyridine case [28]. The results of the calculations given in Table 6 show a more complex situation. Although the predicted energies seem to be slightly overestimated by ∼0.5−1.0 eV, this band may be assigned to three intense transitions, among several low intensity Rydberg transitions. The first one corresponds to the $1s \rightarrow 3p\pi$ transition. Its calculated intensity (9.3%) is unexpectedly high, since there is no N–H* bond which could provide a valence character to the Rydberg transitions and increase the intensity of the band. The two other intense transitions, of B_1 symmetry, are calculated to occur at 404.03 eV and 404.10 eV, with close intensities (11.6 and 15.2%, respectively). Their CI wave-functions are also very similar: about 50% of the $1s \rightarrow 3d\pi$ excitation, with 20% of the $1s \rightarrow 3\pi^*$ and 15% of the $1s \rightarrow 4p\pi$ excitations. Moreover, these two states have also the same $\langle r^2 \rangle$ value (186 and 195 a.u.^{2}). Since the four other 3d transitions are calculated unambiguously to occur in this energy region, it is tempting to assign one of these two states to the $3d\pi$ (B_1) one, while the other would correspond to the $3\pi^*$ transition, which does not appear elsewhere in the calculations. One would therefore expect a low intensity and a large $\langle r^2 \rangle$ value for the Rydberg transition, and the opposite for the valence transition. This is obviously not the case and we have to conclude that it is not possible to label without ambiguity the two states. This is an example of the limit of the mono-electronic description of transitions. It should be reminded that a similar situation occurred at the C1s with the two states calculated at 291.83 and 291.85 eV.

Because of the discrepancy between the calculated transition energies and the maximum of this B band, it is difficult to make a precise assignment. Its asymmetry could indicate that it corresponds to several transitions but could also be due to vibrational excitation. Thus, we tentatively assign the low energy part of this band to the $1s \rightarrow 3p\pi$ transition, while the high energy tail is assigned to the two $1s \rightarrow 3d\pi/3\pi^*$ quasi-degenerate transitions. If this assignment is correct, the calculated intensities are not in agreement with the shape of the band. A possible explanation could be the different lifetimes of these transitions, leading to different widths. However, it is not possible to evaluate these parameters.

The next band C has its maximum at 405.32 eV (Tab. 5) and was assigned by Apen et al. [7] to a double excitation state and the continuum onset. Dudde et al. [30] also proposed a multi-electron state for this feature. The fact that this feature is present in the condensed phase spectrum of Dudde et al. [30] indicates that it cannot be due to Rydberg excitations. The calculations (Tab. 6) predict a large number of low intensity transitions to occur between 404.5 and 406 eV, due to the $n > 3$ Rydberg states, converging to the calculated MP2 ionisation energy (406.14 eV). The energy difference of 0.8 eV could be due to the inaccuracy of the calculations. It is also possible that the continuum onset corresponds to the not-well resolved C' feature, observed at 406.84 eV (Tab. 5). This question could be solved by measuring the core ionisation energy of gaseous s-triazine.

The results of the calculations displayed in Table 6 also confirm the presence of a doubly excited state, calculated at 405.89 eV. Its wave-function is rather complex: $0.13(1s \rightarrow 3\pi^*) + 0.52(1s3\pi \rightarrow 1\pi^*2\pi^*) + 0.18(1s2\pi \rightarrow 2\pi^*3p\pi)$. To clarify the situation, we have used the calculated CI density matrix to obtain the so-called "natural orbitals", as proposed by Löwdin [31]. Such an analysis resulted in four orbitals with an occupation number close to one, confirming the double excitation nature of this state. The calculated $\langle r^2 \rangle$ value of 92 a.u.^{2} shows that it is a valence transition. The most striking result is the calculated intensity: 16.3% of the main peak, which could be sufficient to explain the intensity of the C band if the continuum onset lies at higher energies. A similar high intensity doubly excited state has already been predicted in the K-shell spectrum of benzene [8–32], which is iso-electronic to s-triazine. In the case of benzene, Schwarz et al. [32] placed this state at the continuum onset while our own calculations [8] led us to assign this state to the band observed at 289.09 eV. It is remarkable that the situation is very different at the C1s threshold of s-triazine: the $1s \rightarrow 3\pi^*$ state is mixed mainly with Rydberg excitations and lies well below the ionisation threshold. Another example of doubly excited state is the H_2CO C1s $n \rightarrow \pi^{*2}$ transition predicted to occur just above the C1$s \rightarrow \pi^*$ one with a relative intensity of 0.05% [33]. Doubly excited states around the ionisation threshold have also been predicted in N_2 [34] and their presence has been confirmed experimentally [35]. Triply excited states have also been confirmed [35,36].

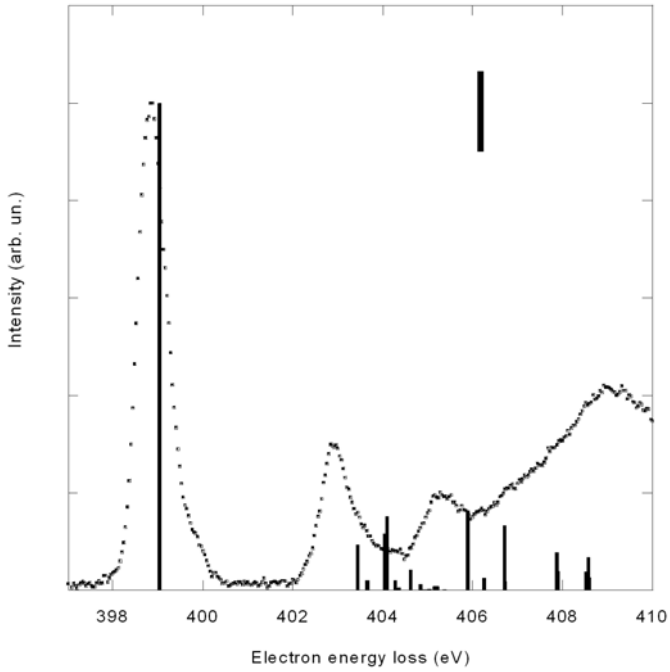

Fig. 5. Comparison of the calculated N1*s* spectrum with the experimental one. The vertical line indicates the calculated ionisation threshold.

The next two bands which can be seen in the experimental spectrum lie at much higher energies (409.10 eV for D and 415 eV for E). As for the C1*s* case, the calculated σ^* and di-excited states shown in Table 6 have only qualitative meaning and are two low in energy. Thus, bands D and E are tentatively assigned to shape resonances. Figure 5 compares the experimental spectrum with the calculated peaks. It appears that the calculations seem to overestimate the core excitation energies by about 0.5 eV.

5 Conclusions

In this work, the inner shell electron energy loss spectra of gaseous *s*-triazine have been measured at the C1*s* and N1*s* edges with 0.17 eV resolution. Accompanying *ab initio* Configuration Interaction calculations using Configuration Interaction have been performed, in order to obtain reliable assignments

At the carbon edge, it appears that the previous assignments of Apen et al. [7] were based on a too low ionisation energy. The present calculations lead to give more precise assignments for some spectral bands and this without ambiguity. At the nitrogen edge, the most important result of the calculations is the presence of an intense doubly excited state predicted to occur below the ionisation threshold, as already observed in the C1*s* spectrum of benzene [8].

At both edges, the calculated wave functions show rather complex patterns, including strong Rydberg-valence character as well as mixing between mono and di-excitations. These results show that in certain cases, a proper description of core electronic transitions requires to go beyond the mono-electronic picture, as done for example in the STEX [37] or GSCF3 [38] approaches. It can be done for example by using Configuration Interaction methods (see for example [14,39], but with a higher computational cost.

The assignments of the K-shell spectra of gaseous *s*-triazine presented in the present work should be useful for the interpretation of core spectra of similar but more complex molecules, such as triazine-based herbicides, either in gas or solid phases. This is of particular importance in the context of soil science, where synchrotron-based spectroscopy has already been used as an analytical technique to detect heterocyclic N compounds [40].

The "Laboratoire de Physique des Lasers, Atomes et Molécules" (PhLAM) is "Unité Mixte de Recherche du CNRS". The "Centre d'Études et de Recherches Lasers et Applications" (CERLA, FR CNRS 2416) is supported by the "Ministère chargé de la Recherche", the "Région Nord/Pas-de-Calais" and the "Fonds Européen de Développement Économique des Régions" (FEDER). Parts of the computations were carried out at the CRI (Centre de Ressources Informatiques), on the IBM-SP3 computer that is supported by the "Programme de Calcul Intensif et Parallèle" of the "Ministère chargé de la Recherche", the "Région Nord/Pas-de-Calais" and the FEDER. This research has been supported by the Fonds National de la Recherche Scientifique and the Patrimoine of University of Liège. M.-J. Hubin-Franskin wishes to acknowledge the Fonds National de la Recherche Scientifique for research position.

References

1. R.T. Meister, C. Sine, *Farm Chemical Handbook* (Meister Publishing Co., Willoughby, OH, 1998)
2. R. Spear, in *Handbook of Pesticide Toxicology*, edited by W.J. Hayes, E.R. Laws (Academic Press, San Diego, 1991)
3. E. Hodgson, P.E. Levi, Environ. Health Perspect. **104**, 97 (1996)
4. H.D. Burrows, M.L. Canle, J.A. Santaballa, J. Photochem. Photobiol. B **67**, 71 (2002)
5. J.M. Oliva, M.E.D.G. Azenha, H.D. Burrows, R. Coimbra, J. Serxio Seixas de Melo, L. Moisés Canle, M. Isabel Fernàndez, J. Arturo Santaballa, L. Serrano-Andrés, Chem. Phys. Chem. **6**, 306 (2005)
6. J. Stöhr, *NEXAFS Spectroscopy* (Springer Verlag, 1992)
7. E. Apen, A. Hitchcock, J. Gland, J. Phys. Chem. **97**, 6859 (1993)
8. D. Duflot, J.-P. Flament, J. Heinesch, M.-J. Hubin-Franskin, J. Electron Spectrosc. Rel. Phen. **113**, 79 (2000)
9. C. Hannay, D. Duflot, J.-P. Flament, M.-J. Hubin-Franskin, J. Chem. Phys. **110**, 5600 (1999)
10. C. Hannay, J. Heinesch, U. Kleyens, M.-J. Hubin-Franskin, Meas. Sci. Technol. **6**, 1140 (1995)
11. M.-J. Hubin-Franskin, H. Aouni, D. Duflot, F. Motte-Tollet, C. Hannay, L.F. Ferreira, G. Tourillon, J. Chem. Phys. **106**, 35 (1997); M.-J. Hubin-Franskin, J. Heinesch, Nucl. Instrum. Meth. Phys. Res. A **477**, 546 (2002)
12. F. Currell, C.M. John, Meas. Sci. Technol. **3**, 1192 (1992)

13. R.N.S. Sodhi, C.E. Brion, J. Electron Spectrosc. Rel. Phen. **34**, 363 (1984)
14. D. Duflot, J.-P. Flament, I.C. Walker, J. Heinesch, M.-J. Hubin-Franskin, J. Chem. Phys. **118**, 1137 (2003)
15. S. Bodeur, P. Millié, I. Nenner, Phys. Rev. A **41**, 252 (1990)
16. M.W. Schmidt, K.K. Baldridge, J.A. Boatz, S.T. Elbert, M.S. Gordon, J.H. Jensen, S. Koseki, N. Matsunaga, K.A. Nguyen, S. Su, T.L. Windus, M. Dupuis, J.A. Montgomery Jr, J. Comp. Chem. **14**, 1347 (1993)
17. B. Huron, J.P. Malrieu, P. Rancurel, J. Chem. Phys. **58**, 5745 (1973); R. Cimiraglia, J. Chem. Phys. **83**, 1746 (1985)
18. C. Angeli, R. Cimiraglia, M. Persico, A. Toniolo, Theor. Chem. Acc. **98**, 57 (1997)
19. T.H. Dunning Jr, J. Chem. Phys. **55**, 716 (1971)
20. T.H. Dunning Jr, P.J. Hay, in *Methods of Electronic Structure Theory*, edited by H.F. Schaefer III (Plenum Press, New York, 1977), Vol. 3, p. 1
21. H. Köppel, W. Domcke, L.S. Cederbaum, Adv. Chem. Phys. **57**, 59 (1984)
22. P.F. Price, E.N. Matsen, W.T. Delany, Acta Cryst. A **34**, 194 (1978)
23. J.E. Lancaster, B.P. Stoicheff, Can. J. Phys. **34**, 1016 (1956)
24. W. Pyckout, I. Callaerts, C. Van Alsenoy, H.J. Geise, A. Almenningen, R. Seip, J. Mol. Struct. **147**, 321 (1986)
25. I.C. Walker, M.H. Palmer, C.A. Ballard, Chem. Phys. **167**, 61 (1992)
26. W.L. Jolly, K.D. Bomben, C.J. Eyerman, At. Data Nucl. Data Tables **31**, 433 (1984)
27. D. Duflot, J.-P. Flament, A. Giuliani, J. Heinesch, M.-J. Hubin-Franskin, J. Chem. Phys. **119**, 8946 (2003)
28. J.A. Horsley, J. Stöhr, A.P. Hitchcock, D.C. Newbury, A.L. Johnson, F.J. Sette, J. Chem. Phys. **83**, 6099 (1985)
29. M.N. Piancastelli, J. Electron Spectrosc. Related Phen. **100**, 167 (1999)
30. R. Dudde, M.L.M. Rocco, E.E. Koch, S. Bernstorff, W. Eberhardt, J. Chem. Phys. **91**, 20 (1989)
31. P.-O. Löwdin, Phys. Rev. **97**, 1474 (1955)
32. W.H.E. Schwarz, T.C. Chang, U. Seeger, K.H. Hwang, Chem. Phys. **117**, 73 (1987)
33. J. Schirmer, A. Barth, F. Tarantelli, Chem. Phys. **122**, 9 (1988); A.B. Trofimov, E.V. Gromov, T.E. Moskovskaya, J. Schirmer, J. Chem. Phys. **113**, 6716 (2000)
34. R. Arneberg, H. Agren, J. Muller, R. Manne, Chem. Phys. Lett. **91**, 362 (1982)
35. E. Shigemasa, T. Gejo, M. Nagasono, T. Hatsui, N. Kosugi, Phys. Rev. A **66**, 022508 (2002)
36. R. Feifel, K. Ueda, A. De Fanis, K. Okada, S. Tanimoto, T. Furuta, H. Shindo, M. Kitajima, H. Tanaka, O. Bjorneholm, L. Karlsson, S. Svensson, S.L. Sorensen, Phys. Rev. A **67**, 032504 (2003)
37. H. Ågren, V. Carravetta, O. Vahtras, L.G.M. Pettersson, Theor. Chem. Acc. **97**, 14 (1997)
38. N. Kosugi, H. Kuroda, Chem. Phys. Lett. **74**, 490 (1980)
39. S. Stranges, M. Alagia, G. Fronzoni, P. Decleva, J. Phys. Chem. A **105**, 3400 (2001)
40. A. Jokic, J.N. Cutler, D.W. Anderson, W.F.L., Can. J. Soil Sci. **84**, 291 (2004)